Eur. Phys. J. B **13**, 745–754 (2000)

THE EUROPEAN PHYSICAL JOURNAL B

EDP Sciences

Thermoelastic behaviour of polyvinylacetate monolayers at the air-water interface: Evidences for liquid-solid phase transition

F. Monroy[1,a], F. Ortega[2], and R.G. Rubio[2]

[1] Laboratoire de Physique des Solides, Bâtiment 510, Université Paris-Sud, 91405 Orsay Cedex, France
[2] Departamento de Química Física I, Facultad de Ciencias Químicas, Universidad Complutense, 28040 Madrid, Spain

Received 12 January 1999 and Received in final form 11 June 1999

Abstract. The thermoelastic behaviour of polyvinylacetate monolayers spread on an aqueous subphase has been studied using rheological data previously published (Monroy *et al.*, Phys. Rev. E **58**, 7629 (1998)). The results show fluid-like viscoelastic behaviour well above a transition temperature $T_{\rm m}$, while at lower temperatures a soft solid-like behaviour emerges. The correlation between thermodynamic and elastic properties below $T_{\rm m}$ can be described in terms of scaling laws.

PACS. 68.10.-m Fluid surfaces and fluid-fluid interfaces – 68.10.Et Interface elasticity, viscosity, and viscoelasticity – 68.60.-p Physical properties of thin films, nonelectronic – 82.65.Dp. Thermodynamics of surfaces and interfaces

1 Introduction

Monomolecular films of small surfactants located at the air-water interface are known to form various solid phases, which have been extensively characterised by different diffraction techniques, particularly grazing incident X-ray from synchrotron sources [1] or neutron diffraction [2]. On the other hand, these quasi-bidimensional systems melt at low surface density and high enough temperature, appearing different fluid phases. In contrast, the low-temperature phases found for monolayers of insoluble polymers do not show, in most cases, crystalline order. In fact, in 3D it is well-known that polymeric systems only form well-defined solid states for some specific tacticities [3]. The presence of chain defects in atactic polymers or polymers with lateral branches, makes it impossible for the polymers to crystallize on cooling, forming amorphous glasses or at most semicrystalline solids. It is commonly accepted that the two generic types of polymeric solids, namely crystalline and glassy polymers, give rise to different elastic states, energy-driven and entropy-driven (rubber-like elasticity), respectively. In the first case, at small strains the displacement of the elastic elements causes a variation in internal energy around the energetic minimum, which corresponds to the equilibrium arrangement in the crystalline lattice, while the entropy remains approximately constant. However, a rubber decreases its internal entropy on elongation, reason for which it recovers its equilibrium dimension if the applied stress ceases. Crystalline order has been however found by Schouten *et al.* [4] in monolayers of PMMA on water if the polymer have a certain degree of tacticity, while the glassy state is the only kinetically accessible phase for the atactic form, as in the 3D system. Furthermore, because of the increase in chain mobility in the monolayer, the loss of a degree of freedom will decrease $T_{\rm g}$ with regards to the 3D value [5,6]. Therefore, polymer concentrated solutions in 2D are excellent candidates to check for fluid-solid transitions in 2D, because, though being basically liquids, normally they behave like highly non-Newtonian viscoelastic fluids, and also under certain circumstances, they seem to behave like a purely elastic solid.

The rheological criterion for distinguishing between a solid and a fluid is that the first exhibits resistance to shear deformation because of the bonding between defects in the solid lattice. In the liquid state at a high enough temperature, it is favourable for the bounded pairs of defects to dissociate because of the resulting gain in entropy. At this point free dislocations appear and the system will respond to a shear stress with no resistance, the mechanism being the continuous creation of dislocation pairs, and pulling them apart to infinity. In these conditions shearing does not store energy in elastic form, only dissipation is present, and we have viscous shear flow [7].

On the other hand, it is well-understood that the character of ordering present in a system depends on its spatial dimensionality [8]. Indeed, it is also generally accepted that because of fluctuations, solids in one or two dimensions lack true long-range order, therefore the melting phenomena is not an expected feature in these systems [8,9]. However, and based in a new definition of

[a] *Permanent address*: Dept. Química Física, Univ. Complutense Madrid.
e-mail: monroy@eucmos.sim.ucm.es

order, so-called "topological order", a theoretical frame for 2D-freezing has been developed by Kosterlitz–Thouless–Halperin–Nelson–Young [10,11]. In the KTHNY theory, the loss of the long-range topological order, renders a melting behaviour essentially different to the tridimensional case. Two-dimensional solids melt *via* sequential continuous phase transition through a hexatic intermediate phase with short-range positional order and quasi-long range bond orientational order. It is also commonly accepted that KTHNY theory of 2D-melting is not based on any particular choice of intermolecular interactions; it remains valid for any system, which can be characterised as a deformable elastic medium [12].

Fluid polymer monolayers [13] can be considered as complex quasi-bidimensional systems, with negligible thickness h, compared with planar dimensions. Hence they behave as very stiff membranes characterised by a set of 2D viscoelastic parameters several orders of magnitude larger than the analogue ones for the bulk system. Particularly, previous studies have demonstrated that polyvinylacetate (PVAc) spread at the air-water interface is able to form very stable monolayers [14–16]. The PVAc atactic chains present extended configurations because of the good-solvent character of the air-water interface for this polymer, which produces a thermodynamic behaviour characterised by very expanded isotherms [14–17]. In a previous paper [18], we have carried out a rheological study of these monolayers in a broad frequency range ($>$ 10 decades) and between 0 and 25 °C. To this end, quasi-elastic surface light scattering (QESLS), excited electrocapillary waves (ECW) and mechanical step-compression experiments were performed.

We have pointed out the strong correlation between the static thermoelastic properties and the dynamic ones, evidencing a high elastic efficiency, which is better at lower temperatures. In addition, a singular behaviour was detected at a temperature around 14 °C, which might be compatible with a transition from a fluid to a soft-solid state. All these issues make this system interesting for checking fluid-solid transitional behaviour in 2D polymeric matter. The results concerning the surface rheology of the PVAc monolayers have been previously described in reference [18]. However, the results were only described from a phenomenological point of view, *i.e.*, no microscopic approach was proposed to explain the observed macroscopic behaviour, unless a chain reptation model was tentatively proposed to explain the complex dynamics found in the low frequency domain. From these data and at surface concentration high enough, the monolayer seems to behave as a quasi-2D polymer gel, made of a network of polymer chains in a near-linear conformation.

The main aim of this work is hence twofold: First, to show clear signatures for the existence of transition from a fluid to a soft-solid state (like a 2D rubber) in the PVAc monolayers as the temperature is decreased. Second, to point out the existence of singular thermoelastic behaviour compatible with bidimensional solidification processes.

The rest of this paper will be organised as follows: Section 2 briefly summarizes the essential concepts of surface hydrodynamics related to our experimental results. Section 3 contains the thermoelastic information derived from the experimental results, and scaling behaviour found for some of the elastic parameters. Finally, Section 4 summarizes the main conclusions.

2 Theoretical background

It is well-known that because of the coupling between transversal and longitudinal motions at the air-water interface, surface hydrodynamics is relevant to the thermoelastic behaviour of polymer films [19]. The transversal or capillary motion is essentially a shear motion, governed by surface tension γ and gravity g, while the longitudinal motion must be decomposed in both, a pure compression mode and a shear mode, characterised by the two different elastic moduli (λ and μ, respectively). Since dissipative effects do exist within the film, each one of these uniaxial moduli must be linearly developed as a viscoelastic response function with imaginary part proportional to a viscosity coefficient. The bulk modulus $\tilde{\varepsilon}$, defined in equation (1), contains both shear μ and compression λ, and it is commonly named dilational modulus. This total longitudinal modulus contains a real part or dilational elasticity ε, and a dissipative term or dilational viscosity $\kappa(=\eta_\mu+\eta_\lambda)$.

$$\tilde{\varepsilon}(T) = \mu(T) + \lambda(T) = \varepsilon + \mathrm{i}\omega\kappa. \tag{1}$$

Although in general the shear contribution to dilational viscosity η_μ, presents non-zero values, it is several orders of magnitude smaller than the compression component η_λ [20,21].

Recently, Buzza *et al.* [22] and earlier Seppecher [23], from rigorous thermodynamic equalities for the viscoelastic free energy functional, have theoretically demonstrated that the transversal dissipation coefficient must be zero in order to obtain a quadratic form for the surface dissipative function, and consequently a minimal dissipation at null deformation [7,22]. In spite that this treatment incorporates new elastic constants related to the spontaneous curvature and its coupling with surface dilatation, they become negligible compared to λ when the interfacial thickness h is small enough as compared with the wavevector, q (*i.e.* $qh \ll 1$). Consequently, the usual hydrodynamic model (see Ref. [19]) with a real and a ω–independent transversal response function equal to the equilibrium surface tension, $\gamma = \gamma_0$ [22], will be valid in the linear viscoelastic regime and for the particular system studied here ($qh \leq 10^{-4}$).

In order to set the meaning of some of the variables used below, it is convenient to briefly review the background associated to the capillary wave experiments. When the hydrodynamic Navier-Stokes equation for oscillatory motion is resolved within the appropriate interfacial boundary conditions, one finds capillary and dilational modes coupled together [19,22,24]. The dispersion equation $D(\omega)$, for this coupled motion finally can be written as:

$$D(\omega) = LT + [\omega\eta(q-m)]^2 = 0 \tag{2}$$

where:

$$L = \tilde{\varepsilon} q^2 + \mathrm{i}\omega\eta(q+m) \tag{3}$$

$$T = \gamma q^2 + \mathrm{i}\omega\eta(q+m) - \frac{\rho}{q}\omega^2 + \rho g \tag{4}$$

m is known as capillary penetration depth in the subphase and is given by:

$$m^2 = q^2 + \mathrm{i}\omega\frac{\rho}{\eta} \quad \text{with} \quad \mathrm{Re}(m) > 0. \tag{5}$$

Solving the dispersion equation for $\gamma = \gamma_0$ and for the propagation characteristics of the surface modes ω, q, one can obtain the dilational parameters $\tilde{\varepsilon} = \varepsilon + \mathrm{i}\omega\kappa$ [18].

3 Results and discussion

3.1 Equilibrium thermoelasticity

The thermodynamic equilibrium properties of the PVAc monolayers spread at the air-water interface have been extensively discussed in detail in a previous work [18]. We will reanalyse here some of the thermoelastic information that will be used later in discussing the solidification-like behaviour.

3.1.1 Concentration regimes and lattice dimension a_0

From the experimental surface pressure-surface concentration ($\Pi - \Gamma$) isotherms we did calculate the critical exponent of the radius of gyration ν for PVAc, and found that it remains constant within the experimental uncertainty at 0.78 ± 0.03 over the whole temperature range [16]. This value is in excellent agreement with the prediction of the Renormalization Group theory for polymers in a bidimensional good solvent [25]. We were also able to calculate the chain overlap concentration Γ^*, which marks the crossover from dilute to semidilute regimes [25]. At this particular concentration the chains begin to overlap and the lateral contact between two independent chains is established. Therefore, one can consider this arrangement as the more compact 2D distribution compatible with the monomer size. Consequently, the area per monomer at $\Gamma^*(A^* = 1/\Gamma^*)$ can be taken as an estimation of the dimensions of a square lattice $a_0^2 \approx A^*$. Figure 1 shows that A^* increases strongly with T, reflecting the tendency of the monolayers to be more expanded at high temperature. Another possible estimation of a_0 can be obtained from the so-called limit area of the isotherm A_{lim}, or surface area of the semidilute regime extrapolated at $\Pi = 0$. In general, these values are smaller than A^*, but as it can be seen in Figure 1, both exhibit the same tendency on increasing T. In these data one observes a clear kink around $14-15\,^{\circ}\mathrm{C}$ which suggests a change in the specific area on cooling the monolayers. This feature will be discussed later in detail.

In order to obtain a good estimation of a_0, continuous compression-expansion cycles in the dilute-semidilute regime ($\Pi < 2$ mN/m) were performed in a Langmuir trough at low enough velocity of the barriers (< 1 mm/min) [14]. No hysteresis processes were detected in these closed cycles. These low Π portions of the isotherms were fitted to the Singer's equation of state (2D version of the configurational lattice model of Flory) corrected with a Van der Waals energetic contribution [26]. This equation is able to describe successfully the diluted portion of the experimental isotherms and from the fits one can obtain a series of microscopic parameters. Particularly the cell dimensions a_0, and the coordination index z of a polymer site in the lattice has been calculated as a function of temperature. The data in Figure 1 show the excellent agreement of the cell parameter $a_0 = \sqrt{A_0}$ calculated from these fits to the equation of state and the area per monomer at Γ^* obtained from the scale analysis in the dilute-semidilute region (see Refs. [14,18] for details). The calculated values for z increase monotonically from a value close to 2 at low temperature to reach an asymptotic limit close to 3.5 at room temperature. In fact, the only admissible values for this parameter are comprised in the range between $z = 2$, value for a fully-extended chain, and $z = 4$ which corresponds to a random coil [33]. The variation observed seems to suggest an internal disorganisation of the chains in increasing temperature from a close to linear to a random-like conformation. This seems to be compatible with the more expanded character of the isotherms (see Ref. [14]), since a random coil excludes more volume than the linear chain of equal molecular weight.

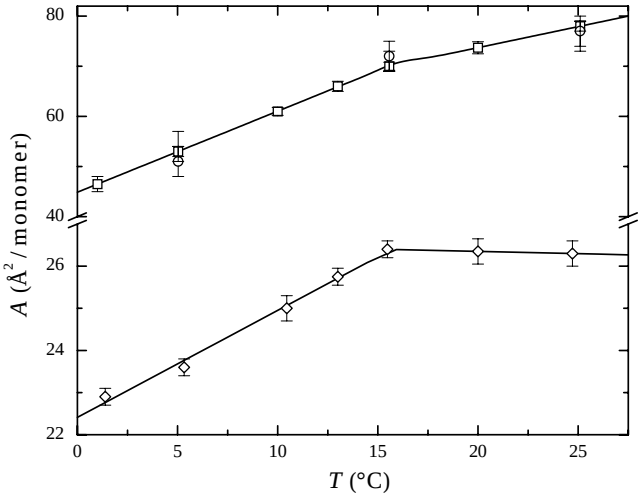

Fig. 1. Temperature dependence of the area per monomer at $\Gamma^*(= 1/A^*)$ (□). For comparison, the cell dimension A_0 obtained from the Singer's equation of state (○) is also represented. (◇) Corresponds to the limit area A_{lim} of the isotherms of the PVAc monolayers.

3.1.2 Thermoelastic properties. Thermal expansivity α and compression ε_0 moduli

It is known that depending on its microscopic configuration, a polymer in 3D may either crystallize or cool

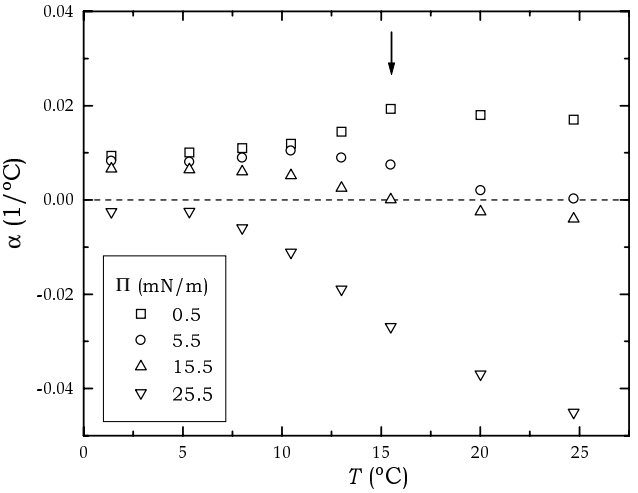

Fig. 2. Thermal expansion coefficient α as a function of T at different surface pressures Π. The arrow marks the hypothetical fluid-solid transition.

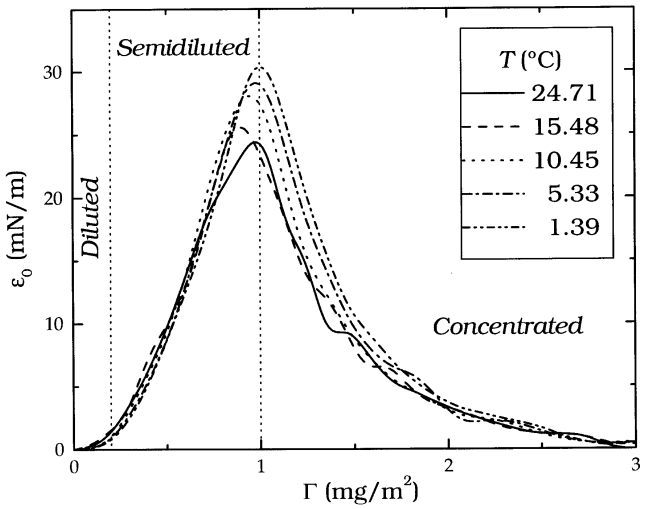

Fig. 3. Static elasticity modulus calculated from the $\Pi-\Gamma$ experimental curves. The dashed lines indicate the limits between the concentration regimes.

down to its glassy amorphous state, but in both cases the thermal expansion coefficient $\alpha = (1/V)(\partial V/\partial T)_P$, varies strongly in crossing the transition temperature [3]. The 2D homologue of this quantity can be calculated from the following expression:

$$\alpha = \frac{1}{A}\left(\frac{\partial A}{\partial T}\right)_{\Pi}. \tag{6}$$

We have calculated α as a function of T from the $\Pi-A$ experimental isotherms [14]. Figure 2 shows that in the low Π regime ($\Pi > 0.5$ mN/m, dilute-semidilute regime) there is a change in the thermal expansivity around 14−15 °C. It is worth noting also the thermal inversion of α in crossing to the concentrated regime at $\Pi \approx 12$ mN/m (and $\Gamma \geq 1$ mg/m^2). Negative values of the thermal expansivity are not a surprising result, in fact there are numerous elastic materials that show contraction upon heating [27]. Negative thermal expansion coefficients have been found by X-ray measurements of the lattice parameters of crystalline and semicrystalline polymers in 3D [27–29]. For example, $\alpha < 0$ is found for cases in which uniaxial orientation is high enough, such as that one found in amorphous extended polymers around or below T_g [27]. As it has been pointed out by several authors [27,29,30], the thermal expansivity of a fully extended chain should be negative because thermal vibrations lead to a shortening of the chain. However, it is important to remark that because of the atacticity of the PVAc, the solid phase speculated here might be more compatible with an amorphous glass than with a crystalline phase, which should be not expected in this system. Similar liquid-solid transition behaviour can be observed by compressing the monolayer at constant temperature, and in fact a similar inversion in α is observed in increasing Π (or Γ). This point has been experimentally corroborated by Armstrong *et al.* [31] in colloidal monolayers, and used by Earnshaw *et al.* [32] to argue the success of KTHNY theory in insoluble monolayers made of small surfactants.

Also, from the experimental $\Pi-\Gamma$ curves of reference [18], it is possible to calculate the more habitual static elasticity modulus λ_0 (or ε_0 in more familiar notation), which accounts only for hydrostatic compression:

$$\varepsilon_0 = \lambda_0 = -A\left(\frac{\partial \Pi}{\partial A}\right)_T = \Gamma\left(\frac{\partial \Pi}{\partial \Gamma}\right)_T. \tag{7}$$

Figure 3 shows ε_0 at different temperatures. It can be observed that most of the increase in the elasticity takes place within the semidiluted regime, where its variation with temperature is almost within the experimental uncertainty. However, near the maximum of elasticity, corresponding to the crossover to a concentrated regime ($\Gamma^{**} \approx 1$ mg/m^2, $\Pi \leq 12$ mN/m), the temperature coefficient of ε_0 becomes negative and non-negligible.

Since ε_0 accounts only for static compression, the data presented in Figure 3 allow one to test for liquid-solid transitional scaling-like behaviour at $T \leq T_m$ in a similar way to the one exhibited by solid monolayers made of small surfactants [32]:

$$\varepsilon_0 = \lambda_0 = \lambda_{T_m} + C_\lambda t^{\Psi}. \tag{8}$$

Figure 4a shows the T-dependence of ε_0 for $\Gamma = \Gamma^{**}$ for the PVAc monolayers. Below $T_m \sim 15$ °C, a strong increase of ε_0 is observed. The fit to the scaling law in equation (8) with $\Psi = 0.37$ follows quite good the experimental data for $T < T_m$ using $T_m = 14.9 \pm 0.4$ °C, $\lambda_0(T = T_m) = \lambda_0 = 23.2 \pm 0.6$ mN/m and $C_\lambda = 7.2 \pm 0.9$ mN/m. It must be remarked that the KTHNY theory leads to equation (8) with $\Psi = 0.37$. However, it is worth noting that the experimental data around T_m show a smoother trend that expected for pure hexatic-fluid transitional behaviour.

We have also tried to fit the data with Ψ variable and T_m fixed, since there is a strong correlation between both parameters. Table 1 collects these parameters for several

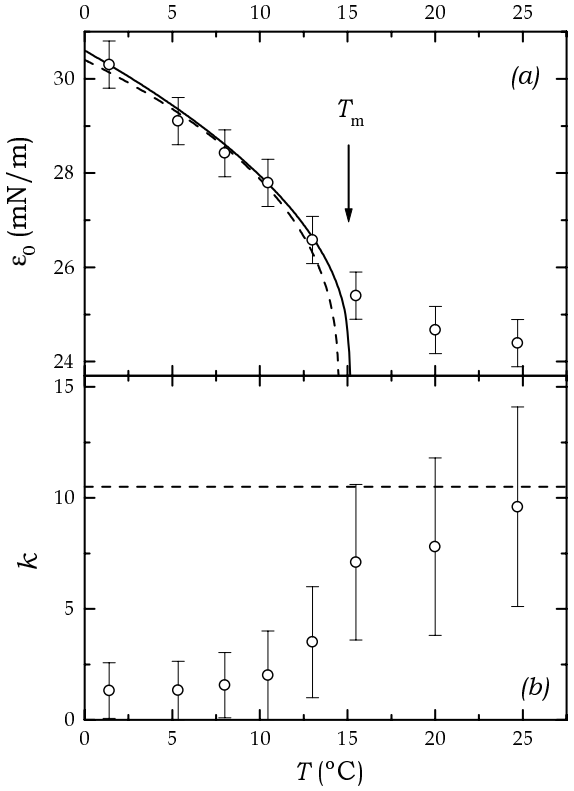

Fig. 4. (a) T-dependence of ε_0 at $\Gamma = \Gamma^{**}$ and verification of scaling behaviour at $T \leq T_m$: (—) $\Psi = 0.52$ and (- - -) $\Psi = 0.37$ (see parameters in Tab. 1). (b) Experimental verification of the Struik's relationship between the temperature coefficient of the 2D static elasticity modulus ε_0 and the thermal expansivity α (see Eq. (9)) at $\Gamma = \Gamma^{**}$.

Table 1. Fitted values of the parameters in equation (8) at different fixed values of T_m.

T_m (°C)	C_λ (mN/m)	Ψ	λ_{T_m} (mN/m)
15.0	6.1 ± 1.3	0.52 ± 0.15	24.5 ± 1.5
14.9	6.4 ± 1.7	0.47 ± 0.20	24.1 ± 2.0
14.8	6.8 ± 1.8	0.41 ± 0.18	23.6 ± 2.0
14.5	7.2 ± 1.2	0.37 ± 0.15	23.2 ± 1.4

values of T_m. Because of the experimental uncertainty, it is evident that these fits do not allow clearly elucidate between $\Psi = 0.5$ and $\Psi = 0.37$. A tendency toward $\Psi = 0.37$ is detected also in decreasing weakly T_m in the fits. As it can be seen in Figure 4a, the validity range for simple scaling is remarkably large: the data follow the scaling predictions within the experimental error at the lowest T, ($T_m - T \sim 15\,°C$). This might be interpreted as a strong influence of the critical fluctuations onto the elastic properties of the solid network, even at temperatures far from T_m.

From the point of view of the equilibrium elasticity [7], the static elasticity modulus does not include any dissipation. Consequently, the decrease of ε_0 of the solid as T increases reflects the direct influence of the thermal expansion in elastic behaviour. In fact, positive values of α correspond to expanded polymer chains and more as T increases, consequently the energy-driven contribution to the elasticity will vanish at high enough temperature [27]. Furthermore, Struik [27] has found the following empirical relation between the thermal expansivity and the temperature coefficient of the elasticity modulus:

$$-\frac{1}{E}\left(\frac{\mathrm{d}E}{\mathrm{d}T}\right) \approx k\alpha \tag{9}$$

where $k \approx 10.5$ for a variety of 3D polymeric amorphous systems. By using the calculated values of α and the temperature coefficient of ε_0 at the Γ^{**} state (close to the maximum of elasticity), calculated by numerical derivation of the data in Figure 6a, we have verified the validity of this relationship in the quasi-2D system considered here. Figure 4b shows the calculated values of the proportional constant k in equation (9). The agreement with the expected value is quite good at $T \geq T_m$ (≈ 14–$15\,°C$), while at T below the melting temperature an increasing negative difference is clearly observed. These data correlate well with the picture of a rubber-like elastic film at high T, which deviates toward a different solid state at $T \leq T_m$.

3.1.3 Nature of the solid phase. Enthalpic and entropic content

From the experimental isotherms, entropy Δs and enthalpy Δh excesses with respect to the bare surface of the liquid subphase can be calculated. It has been found that both Δs and Δh decrease monotonically with T in all surface states. Particularly, states with $\Delta s < 0$ over the whole T range are found at $\Gamma \geq \Gamma^{**}$ (≈ 1 mg/m^2), which indicates the higher degree of order of the monolayers formed in the concentrated regime compared to the free surface of the aqueous subphase. The formation process of these concentrated surface states is exothermic in nature ($\Delta h < 0$), pointing out their high thermodynamic stability. The ratio between the entropic f_S and energetic f_E contributions to the total elastic force f, under constant area conditions is given by [3]:

$$\frac{f_S}{f_E} = \frac{\dfrac{T}{\varepsilon_0}\left(\dfrac{\partial \varepsilon_0}{\partial T}\right)_A}{1 - \dfrac{T}{\varepsilon_0}\left(\dfrac{\partial \varepsilon_0}{\partial T}\right)_A}\,. \tag{10}$$

This ratio must correlate with the ratio between the energetic and entropic contributions to the total free energy of the monolayer:

$$\frac{f_S}{f_E} \sim \frac{\Delta s}{\Delta h + T\Delta s}\,. \tag{11}$$

The quantity in equation (10) has been calculated in the reference state $\Gamma = \Gamma^{**}$ and it has been compared with the energetic-to-entropic ratio expressed in equation (11).

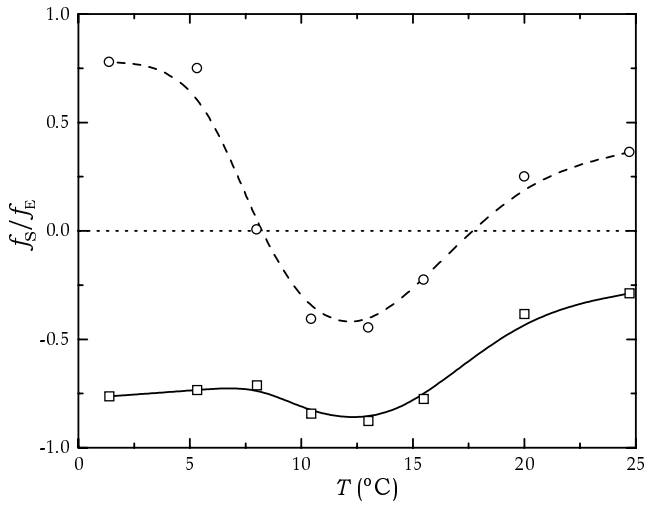

Fig. 5. Relative contribution of the energetic f_E and entropic f_S terms to the total elasticity, (□) calculated from the exact formula in equation (10), and (○) from the ratio between the variation of entropy and free energy in the monolayer formation process (see Eq. (11)).

Figure 5 shows the correlation between the elastic and thermodynamic calculation. In fact, a minimum appears at the same temperature, around 13 °C, which could be associated to the effectiveness of the entropic contribution, at temperatures just below T_m, to promote the solid-fluid transition. Since $|f_S/f_E| < 1$, the dominance of the energetic contributions can be inferred. Moreover, the negative values of this ratio is an indirect signature of the near-to-fully-extended configuration of the polymer chains as it has been earlier emphasised. Particularly, the statistical micromechanical theory of rubber elasticity developed by Flory and Rehner [33], predicts a direct relationship between the energetic contribution f_E and the end-to-end distance as follows:

$$f_E \sim T \frac{d \ln \langle r^2 \rangle_0}{dT} . \quad (12)$$

In fact, in discussing the α data (see Fig. 2), we have already mentioned that only a nearly fully-extended configuration allows contraction in heating the system. Only in this particular case, negative values of f_E have been described. This point has been extensively corroborated in polymers in 3D. More precisely, by using mechanical dilatometry, Mark [3] has obtained negative values in linear polyethylene. Therefore, the observed thermoelasticity is compatible with a energy-driven mechanism, as a consequence of the extended configuration of the PVAc chains at the air-water interface.

3.2 Surface viscoelasticity

Mechanical step-compression experiments (MSC) on PVAc monolayers have been carried out at different temperatures near the $\Gamma = \Gamma^{**}$ surface state. As it has been shown in a previous study [18], this system exhibits a complex viscoelastic relaxation over several decades in frequency. The experimental relaxation spectra $H(\ln \tau)$ are a discrete sequence of broadened Gaussians (Maxwell modes) with a series of characteristic relaxation times in good agreement with the normal modes structure predicted by a 2D reptation model recently proposed by Noskov [34]. At higher frequencies, by combining electrocapillary excited waves (ECW) (20 Hz–3 kHz) and SQSLS (10 kHz–200 kHz) techniques, it has been shown that a series of independent diffusion modes do exist (see Ref. [18] for a more detailed description). In order to explain briefly the reasons to conjecture transitional behaviour from the low ω data, Figure 6 shows the reptation relaxation times as a function of T, where it is easy to observe a clear discontinuity in the slowest relaxation time.

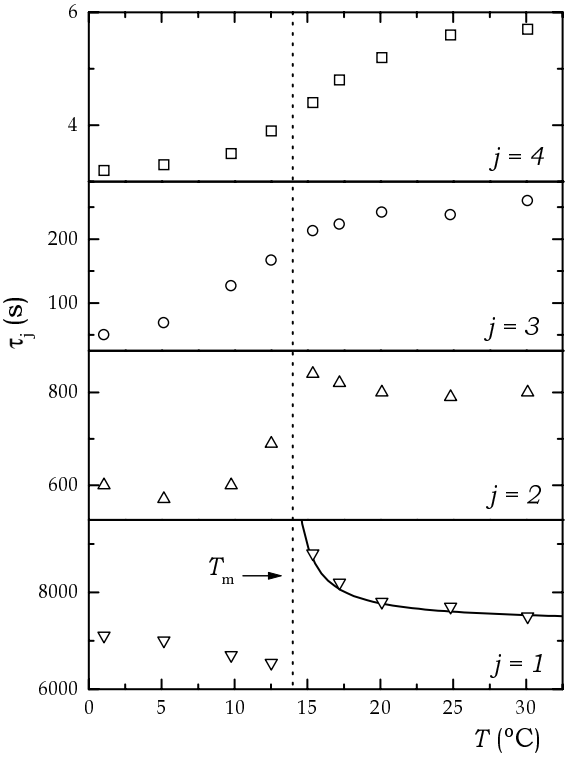

Fig. 6. Low-ω relaxation times obtained from step-compression experiments. The entire number j reads to a reptation normal mode in the Noskov's theory; τ at $j = 1$ is the director relaxation time of this reptation dynamics. The continuous line in the slowest data ($j = 1$) represents the fit to the WLF equation.

As it has already been demonstrated in reference [18], the T-dependence of these low frequency data follows the WLF equation, and the discontinuous jump in the director time of the reptation dynamics τ_1 is predicted at $T = T_m = 14 \pm 1$ °C. Keddie *et al.* [5] have found that the T_g of thin films of PMMA and PS deposited on solid substrates is smaller than for bulk samples. The bulk T_g of our PVAc sample is 44 °C, thus the transition found at $T_m = 14$ °C might be associated to the T_g of the quasi-2D system considered here. Moreover, the observed discontinuity at low ω progressively vanishes as

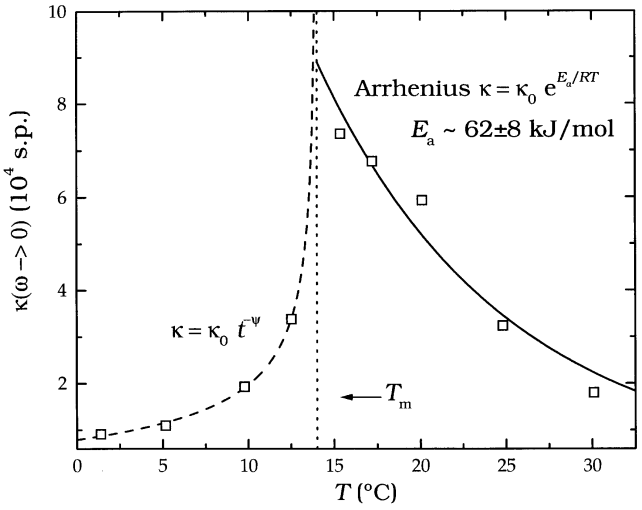

Fig. 7. T-dependence of the static limit of the dilational viscosity κ. Above T_m Arrhenius-like behaviour (—) with activation energy $E_a \sim 62$ kJ/mol is found. Below T_m a divergent power-like behaviour is found (- - -).

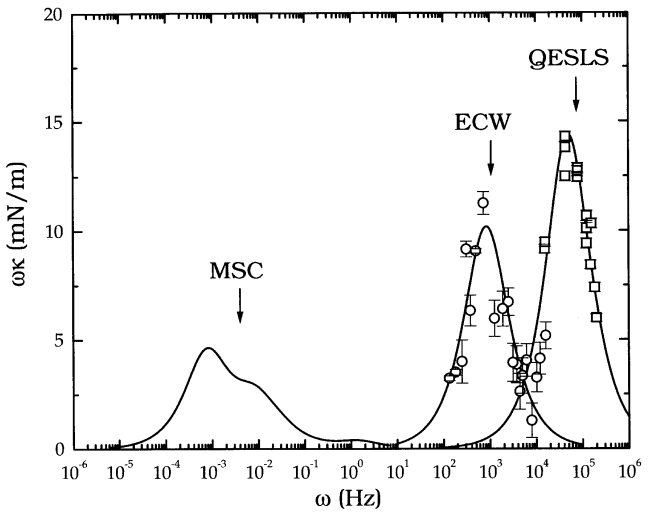

Fig. 8. Frequency dependence of the dilational loss modulus $\omega\kappa$ of a PVAc monolayer of $\Gamma = \Gamma^{**}$ at 25 °C. The results have been obtained by combination of mechanical step-compression (MSC) experiments, electrocapillary waves (ECW) and surface light scattering (QESLS).

the motion become faster, suggesting the no existence of transitional fluctuations at high ω. In fact, the light scattering data (~ 25 kHz) at the same surface concentration confirm the total disappearance of the WLF T-dependence of the relaxation time for the high ω motion, which, in contrast, becomes Arrhenius-like with high activation energy ($E_a \sim 87$ kJ/mol) [18].

3.2.1 Dilational viscosity

Here, we are only interested in asymptotic viscoelastic behaviour, as free as possible of relaxation effects, therefore, only the zero-frequency limit of the low ω data will be discussed in detail. Figure 7 shows the T-dependence of the static limit of the dilational viscosity $\kappa(\omega \to 0)$ calculated from the data in reference [18]. A divergence is observed in $\kappa(\omega \to 0)$ around $T_m \sim 14\,°C$. Below T_m, a strong increase with T is detected in approaching the transition point. The experimental points have been fitted to an empirical power law $\sim t^{-\beta}$ with $t = (T_m - T)/T_m$. Fixing $T_m = 14.0\,°C$, one obtains a good quality fit with $\beta = 0.37 \pm 0.05$ as in the previous section (see Fig. 4). Above the transition, a smoother decrease of κ on increasing T is observed. This variation follows the Arrhenius law, as expected for the molten state. The calculated value for the activation energy $E_a = 62 \pm 8$ kJ/mol is slightly lower than the high-ω value ($E_a = 87$ kJ/mol) obtained from the light scattering data [18]. This means that the energetic cost of pulling apart two contiguous frictioning elements in the monolayer is lower for the slowest motion, evidencing synergism in the long-range interactions, responsible for the collective character of the reptation molecular motions. This is compatible with the spectrum shown in Figure 8. As it can be observed, the area subtended by the different relaxation process increases with log ω which indicates that the total viscous dissipation grows exponentially at high ω.

3.2.2 Dilational and shear elasticity

In order to check for solid-like elastic behaviour, it would be necessary to obtain simultaneously the two dilational elastic moduli, compression λ and shear μ. The problem is that the bulk modulus $\tilde{\varepsilon}(\omega)$ involved in the dispersion equation contains these two moduli coupled together. However, and since the static elasticity modulus $\lambda_0 = \varepsilon_0$ only contains hydrostatic compression, it would be possible to discriminate the partial contribution of the shear component to the total dilational modulus if the further increase in $\lambda(\omega)$ due to internal viscoelastic relaxation was considered. For insoluble monolayers, the excess in the dilational modulus at high frequency $\tilde{\varepsilon}(\omega)$ with respect to the static value ε_0, is due to two simultaneous and independent factors: relaxation and shear effects. Frequently, shearing effects are not considered because of the fluid character of the more usual monolayers, but for a solid monolayer they should be taken into account. Therefore, and assuming a Maxwell-like relaxation [35], the expected ω-functionality of the dilational modulus is given by:

$$\tilde{\varepsilon}(\omega) = \mu + \lambda_0 + \Sigma_k \lambda_k \frac{\omega^2 \tau_k^2}{1 + \omega^2 \tau_k^2} \qquad (13)$$

where λ_k accounts for the amplitude of the different relaxation process that could exist, which, if the strain is small enough and the system is in the linear viscoelastic regime, should only produce adsorption or desorption of a small fraction $\beta = \delta\Gamma'/\delta\Gamma_{eq} \ll 1$, of the total amount of monomers involved in a static compression, $\delta\Gamma_{eq}$.

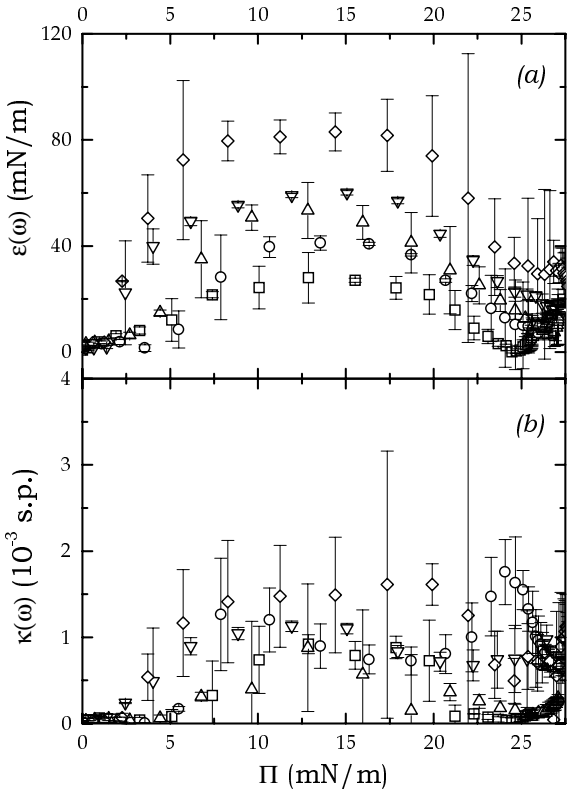

Fig. 9. High frequency total dilational viscoelastic parameters $\tilde{\varepsilon}(\omega)$ (shear plus compression) of PVAc monolayers at different temperatures: (a) elastic or store modulus $\varepsilon(\omega)$ and (b) total dilational viscosity $\kappa(\omega)$.

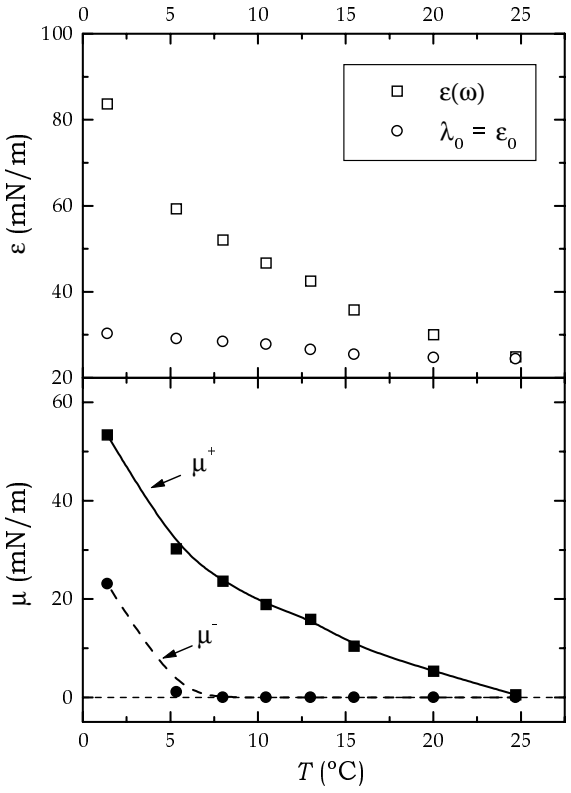

Fig. 10. (a) T-dependence of the elasticity modulus at $\Pi = 12$ mN/m $\sim$ Γ^{**}, (□) total elasticity $\varepsilon(\omega) = \lambda + \mu$ at $q = 229.6$ cm^{-1}, and (○) static compression modulus λ_0. (b) Estimated upper (μ^+) and lower (μ^-) limits for the shear component of the elastic modulus (see Eq. (15)).

In the case of a small uniaxial dilation $\theta_\lambda = \delta\Gamma_{\rm eq}/\Gamma_{\rm eq}$, a total stress relaxation is therefore observed, $\delta\Pi(\omega) = \delta\Pi_{\rm eq}(\delta\Gamma_{\rm eq}) + \delta\Pi' = \varepsilon(\omega)\theta_\lambda$. In the linear regime, which is the case of hydrodynamic motion induced by surface modes or the small deformations involved in the MSC experiments, one has $\delta\Pi' \approx (\partial\Pi/\partial\Gamma)\delta\Gamma' = \lambda_0(\delta\Gamma'/\Gamma_{\rm eq})$, and $\varepsilon(\omega) \approx \lambda_0(1+\beta)$. Therefore, it does not seem too plausible that the additional relaxations increase the elastic modulus more than the static elasticity itself. Consequently, and following the above argument, there will be a maximum limit for the relaxation component to the compression modulus:

$$\Sigma_k \lambda_k = \beta\lambda_0 \leq \lambda_0 \tag{14}$$

from which the range for the shear component can be written as:

$$\mu^+ = \tilde{\varepsilon}(\omega) - 2\lambda_0 \geq \mu \geq \mu^- = \tilde{\varepsilon}(\omega) - \lambda_0. \tag{15}$$

Therefore, at least an estimation of the shear modulus can be given if one knows the dilational modulus at frequencies high enough. Figure 9 shows the results for dilational viscoelastic modulus at high frequency (~ 25 kHz QESLS) at some of the measured temperatures. In order to compare surface states with equivalent energy-driven elasticity, the Π = constant thermodynamic path has been chosen. At low $\Pi(\leq 2\,\text{mN/m})$, $\tilde{\varepsilon}(\omega)$ is small and remains constant with Π over the whole temperature range. In a similar way to the static modulus, $\tilde{\varepsilon}(\omega)$ grows suddenly in the semidiluted regime until it reaches a maximum value at $\Pi = \Pi^{**} \sim 12$ mN/m [$\Gamma(\Pi^{**}) \sim \Gamma^{**} \sim 1$ mg/m^2], which is always higher than the static value at the same Π. However, it is worth noting that while at high T this difference is small, at temperature low enough, the maximum elasticity value increases strongly with regard to the static value. At $T = 1.35\,^\circ$C one has $\varepsilon_0 = 27.0$ mN/m and $\tilde{\varepsilon}(\omega) = 83.70$ mN/m, *i.e.*, between 30 and 57 mN/m of this total amount (36–68%) corresponds to the shear component. The experimental values of the dilational viscosity κ, shown in Figure 9b, vary with Π (or Γ) in a similar way than $\tilde{\varepsilon}(\omega)$. Its T-dependence is less clear, remaining almost constant within the experimental error. Figure 10 shows both, the high-ω elasticity modulus and the static value at $\Pi = 12$ mN/m. The range of variation of μ, calculated from equation (15) have been also included. Since negative values for μ^- are physically meaningless they have been made equal to zero. The kink in the slope of the $\tilde{\varepsilon}(\omega)$ data in Figure 10a is less clear than for the static ones λ_0, (see Fig. 4a, also) on one side due to its greater absolute variation and, on the other side because of an eventual q-induced $T_{\rm m}$-drift to higher temperatures. However, the concavity of $\tilde{\varepsilon}(\omega)$ at $T \leq T_{\rm m}$ (static conditions $\sim 15\,^\circ$C), does not seem compatible with a scaling behaviour with

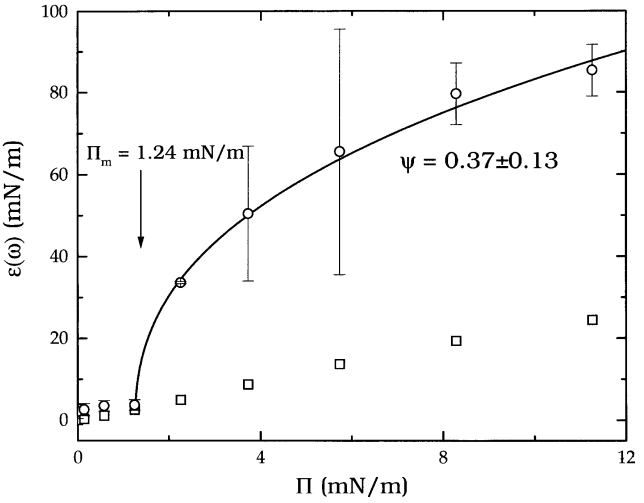

Fig. 11. Scaling behaviour in the total elasticity coefficient $\tilde{\varepsilon}(\omega)$ (○) in a melting by compression process. Comparison with the static compression modulus λ_0 (□). The continuous line represents the fit to the scaling law in equation (16) with the exponent $\Psi = 0.37$.

a critical exponent Ψ lower than unity. Figure 10b shows a clear tendency to fluid-like behaviour ($\mu \to 0$) at temperatures high enough. Clearly, the data at the lowest temperatures are compatible with a certain minimum amount of shear component, which confirms that these states behave like a 2D solid.

A similar behaviour should be found in a solidification process carried out by an isothermal compression path. As it has been discussed in Section 3.1.3, the PVAc monolayers seem to behave according to an energy-driven elastic mechanism, consequently the compression path must be a more evident *via* for surface freezing than the thermal cooling (entropic in nature). In practice, T must be replaced by Π, and if the film undergoes a melting process under expansion, the elastic modulus $\tilde{\varepsilon}(\omega)$ should strongly decrease at $\Pi = \Pi_{\rm m}$. The success of equation (8) lead us to consider that the elastic coefficient might follow a scaling law in the reduce pressure, $\Pi_{\rm R} = (\Pi - \Pi_{\rm m})/\Pi_{\rm m}$:

$$\varepsilon \sim \Pi_{\rm R}^{\Psi} \tag{16}$$

with $\Psi = 0.37{-}0.5$.

This correspondence has been earlier recognized by Earnshaw *et al.* [32] in small surfactants monolayers, which can exhibit true hexatic mesophases at monomeric specific area and temperature low enough, and where the KTHNY theory might hence apply successfully [32]. Also we think that since Π, instead of A, is the generalised force associated to the 2D mechanical work, it would be the rigorous mechanical equivalent of T for the isothermal compression path.

Figure 11 shows the low Π portion of the $\varepsilon{-}\Pi$ curve at $T = 1.35\,^{\circ}$C. Similar results have been found at the rest of temperatures studied at $T < T_{\rm m}$. In this figure it is easy to see the abrupt change in the elasticity coefficient at $\Pi = \Pi_{\rm m}$. At lower pressures ($\Pi \leq \Pi_{\rm m} \sim 1.24$ mN/m, in the diluted regime), the total elasticity $\tilde{\varepsilon}(\omega)$ values are close to the compression ones, $\lambda_0 = \varepsilon_0$, and close to zero as corresponds to a fluid phase. At $\Pi = \Pi_{\rm m} \sim \Pi^*$, the total bulk modulus $\tilde{\varepsilon}(\omega) = \lambda(\omega) + \mu(\omega)$ grows suddenly while the static compressibility λ_0 remains in a low value ($\mu \gg \lambda \sim 0$). This is compatible with the idea of a more organized phase at lower temperature, with the polymer chains in a near fully-extended configuration. Under such conditions it would be rather difficult to deform the monolayer by compression ($\lambda \sim 0$). This transitional behaviour at the crossover to the semidiluted regime ($\Pi \geq \Pi_{\rm m} \sim \Pi^*$) is compatible with the scaling law in equation (16) with critical exponent $\Psi = 0.37 \pm 0.13$ in the proposed melting by expansion process, corroborating hence the existence of a solid shearing phase at $\Pi \geq \Pi_{\rm m}$ and $T \geq T_{\rm m}$.

4 Conclusions

The thermoelastic behaviour of PVAc monolayers has been reanalysed from the rheological data already published in a earlier paper, pointing out the existence of transitional behaviour around $T_{\rm m} \sim 14\,^{\circ}$C. Above this temperature a viscoelastic fluid phase exists like a 2D-gel. Below $T_{\rm m}$, a solid-like behaviour emerges, conjecturing about a glass network made of crosslinked extended chains. In particular, scaling-like behaviour has been found in the viscoelastic coefficients of the solid phase at temperatures below $T_{\rm m}$. Singular behaviour of the bulk modulus has been also evidenced in a freezing by compression process; a strong increase of the elastic modulus is observed in crossing from the fluid state to the solid, which points out that a shear contribution $\mu \neq 0$ emerges over the total bulk modulus $\tilde{\varepsilon} = \lambda + \mu$, as expected for a 2D-solid. Finally, from the global thermoelastic equilibrium behaviour of the PVAc monolayers, the dominance of energetic effects in the elastic response has been inferred, in contrast with the more usual entropic mechanism responsible for rubber elasticity in amorphous materials. An extended-like configurational image, compatible with the experimental $\Pi{-}A$ isotherms, has been tentatively conjectured for the PVAc chains at the air-water interface. This can explain the observed thermoelastic behaviour, particularly the thermal contraction ($\alpha < 0$) found in the solid state, opening the possibility for solid-like behaviour; a network of defects, with a fair degree of long-range order, in a matrix made of crosslinked full extended chains could be formed at low temperature and high surface density.

F. Monroy thanks Centre d'Études de Physique Théorique et Nucléaire (CEPHYTEN France) for financial support under contract 98/44-Rhône Poulenc. This work was supported in part by Fundación Ramón Areces and by DGES under grant PB96-609.

References

1. R.M. Kenn, C. Böhm, A.M. Bibo, I.R. Peterson, H. Möhwald, J. Als-Nielsen, K. Kjaer, J. Phys. Chem. **95**, 2092 (1991).
2. J.E. Bradley, E.M. Lee, R.K. Thomas, A.J. Willatt, J. Penfold, R.C. Ward, D.P. Gregory, W. Waschowsky, Langmuir **4**, 821 (1988).
3. U.W. Gedde, *Polymer Physics* (Chapman & Hall, London, 1995).
4. R.H.G. Brinkhuis, A.J. Schouten, Macromolecules **24**, 1496 (1991); *ibid.* **25**, 5683 (1992); *ibid.* **25**, 5692 (1992).
5. J.L. Keddie, R.A.L. Jones, R.A. Cory, Faraday Discuss. **98**, 219, (1994); Europhys. Lett. **27**, 59 (1994).
6. J.A. Forrest, K. Dalnoki-Veress, J.R. Stevens, J.R. Dutcher, Phys. Rev. Lett. **77**, 2002 (1996).
7. L.D. Landau, E.M. Lifshitz, *Theory of the Elasticity* (Pergamon, Oxford, 1986).
8. L.D. Landau, E.M. Lifshitz, *Statistical Physics* (Pergamon, Oxford, 1986).
9. N.D. Mermin, J. Math. Phys. **8**, 1061 (1967); Phys. Rev. **176**, 250 (1968).
10. J.M. Kosterlitz, D.J. Thouless, J. Phys. C **6**, 1181 (1973).
11. For a review, see D.R. Nelson, in *Phase Transitions and Critical Phenomena*, Vol. 7, edited by C. Domb, J.L. Lebowitz (Academic, London, 1983).
12. R. Zangi, S. Rice, Phys. Rev. B **58**, 7529 (1998).
13. M. Kawaguchi, Prog. Polym. Sci. **18**, 341 (1993).
14. F. Monroy, M.J. Esquinas, F. Ortega, R.G. Rubio, Colloid Polym. Sci. **276**, 960 (1998).
15. K.W. Yoo, H. Yu, Macromolecules **22**, 4019, (1989).
16. B.B. Sauer, H. Yu, M. Yazdanian, G. Zogafri, M.M. Kim, Macromolecules **22**, 2332 (1989).
17. F. Monroy, F. Ortega, R.G. Rubio, J. Phys. Chem. **103**, 2061 (1999).
18. F. Monroy, F. Ortega, R.G. Rubio, Phys. Rev. E **58**, 7629 (1998).
19. L. Kramer, J. Chem. Phys. **55**, 2097 (1971).
20. H.C. Maru, D.T. Wasan, Chem. Eng. Sci. **34**, 1295 (1979).
21. F. Monroy, J. Giermanska-Kahn, D. Langevin, Colloids Surf. **143**, 251 (1998).
22. D.M.A. Buzza, J.L. Jones, T.C.B. McLeish, R.W. Richards, J. Chem. Phys. **109**, 5008 (1998).
23. P. Seppecher, Ph.D. thesis, Pierre et Marie Curie University, Paris, 1987.
24. E.H. Lucassen-Reynders, J. Lucassen, Adv. Colloid Interf. Sci. **2**, 347 (1969).
25. P.G. de Gennes, *Scaling Concepts in Polymer Physics* (Cornell Univ. Press, Ithaca, NY, 1979).
26. S.J. Singer, J. Chem. Phys. **16**, 872 (1948).
27. L.C.E. Struik, *Internal Stresses, Dimensional Instabilities and Molecular Orientations in Plastics* (Wiley, Chichester, 1990).
28. C.L. Choy, S.P. Wong, K. Young, J. Polym. Sci. (Phys.) **22**, 979 (1984).
29. L.C.E. Struik, Polymer Eng. Sci. **18**, 799 (1978).
30. C.L. Choy, in *Developments in Oriented Polymers-1*, edited by I.M. Ward (Appl. Sci. Publ., London, 1982).
31. A.J. Armstrong, R.C. Mockler, W.J. O'Sullivan, J. Phys. Cond. Matter **1**, 1707 (1989).
32. D. Sharpe, J.C. Earnshaw, K. Haig, Y. Li, Phys. Rev. B. **55**, 6260 (1997).
33. P. Flory, J. Rehner, J. Chem. Phys. **11**, 512, (1943).
34. B.A. Noskov, Colloid Polym. Sci. **273**, 263 (1995).
35. J.L. Harden, H. Pleiner, Phys. Rev. E **49**, 1411 (1994).